International Journal of Multiphase Flow 131 (2020) 103351

Contents lists available at ScienceDirect

International Journal of Multiphase Flow

journal homepage: www.elsevier.com/locate/ijmulflow

Development of Delayed Equilibrium Model for CO_2 convergent-divergent nozzle transonic flashing flow

Wojciech Angielczyk[a], Yann Bartosiewicz[b], Dariusz Butrymowicz[a,*]

[a] Bialystok University of Technology, Wiejska 45C, Bialystok, 15-351, Poland
[b] Université catholique de Louvain (UCLouvain), Institute of Mechanics, Materials and Civil Engineering (iMMC), Thermodynamics and fluid mechanics division (TFL), Place du Levant 2, 1348 Louvain-la-Neuve, Belgium

ARTICLE INFO

Article history:
Received 26 December 2019
Revised 13 May 2020
Accepted 14 May 2020
Available online 25 May 2020

Key words:
Convergent-Divergent Nozzle
Ejector Nozzle
Two-Phase Flow
Critical Mass Flow Rate
Thermal Non-Equilibrium
Friction Factor
Vaporization Index Evolution
Carbon Dioxide

ABSTRACT

The one-dimensional implementation of the Delayed Equilibrium Model (DEM) is known as a relatively simple yet accurate approach for prediction of critical mass flow rate, pressure and void fraction distributions for two-phase water transonic flows in ducts of variable geometry. However, the direct application of DEM equipped with original saturation index evolution law and Lockhart-Martinelli approach (the original setup) is incapable of accurate prediction of CO_2 transonic flow. Moreover, the Darcy friction factor approach has a significant impact on the simulation results. Consequently, this paper presents a new law of the saturation index evolution and a new frictional pressure gradient approach for CO_2 transonic two-phase flows together with experimental validation and discussion of obtained data. A comparative analysis of the developed DEM setup and the referential Homogeneous Equilibrium Model revealed that application of the proposed approaches decreases the mean maximal discrepancy between experimental and calculated static pressure values by a factor of app. 2, with simultaneous decrease of the standard deviation by a factor of app. 4. That proves that both the frictional pressure gradient approach and the proper introduction of the thermal non-equilibrium effects are substantial for accurate modelling of the flashing process in CO_2 flows.

1. Introduction

Flashing is a phenomenon of intensive evaporation in flowing liquid due to a decrease in static pressure. The process of the vapour phase generation is usually accompanied by significant thermodynamic and mechanical non-equilibrium, which is mainly manifested by a difference in temperature and velocities of the phases. This article focuses on the flashing process that occurs in the flow through a convergent-divergent nozzle that is a part of a two-phase ejector. The schematic of the two-phase ejector with supercritical or subcooled liquid phase as a motive fluid and with a vapour phase as a secondary fluid is presented in Fig. 1a. The liquid phase due to depressurisation achieves saturation conditions and partly evaporates inside the motive nozzle so that two-phase flow emanates from the nozzle. Due to momentum transfer between the motive jet and the vapour, the vapour is entrained into the suction chamber and further into the mixing chamber. The progressing momentum transfer causes a mixing process that takes place together with formation of a two-phase shock wave. The appearance of the shock wave dramatically rises the static pressure of the mixture. Finally, the homogeneous two-phase mixture is additionally compressed in the diffuser achieving the discharge pressure p_m, which is higher than the pressure of the entrained vapour p_0.

A more detailed insight into the flashing process that occurs in the convergent-divergent nozzle is presented in Fig. 1b. The supercritical or subcooled liquid enters the motive nozzle and partly evaporates (mostly due to accelerational depressurisation). The rate of evaporation at the beginning of the flashing flow depends on two factors: the number of active nuclei and the superheat of liquid. However, the smaller nucleus the higher superheat is required for its activation. Therefore, despite that at a certain location, the equilibrium saturation pressure is achieved, the vaporization process does not start and a metastable liquid flow occurs up to a location where the metastable liquid is sufficiently superheated to activate the largest nuclei, Boure et al. (1976). From that location, the two-phase flashing flow is formed and the vapour phase growth rate is limited by the interphase heat transfer rate rather instead of mechanical expansion. However, under real operation conditions, both mechanical and thermal non-equilibrium exist simultaneously during flashing process inside the

* Corresponding author.
E-mail address: d.butrymowicz@pb.edu.pl (D. Butrymowicz).

https://doi.org/10.1016/j.ijmultiphaseflow.2020.103351
0301-9322/

Symbols

A	flow channel cross-section surface area, m^2
A_{ij}	coefficient matrix of eq. system (14)
a_1, a_2	functions defined in eq. (28) and eq. (29)
a_{g1}, a_{g2}	constants defined in eq. (29)
b	function defined in eq. (34)
b_i	source terms vector of eq. system (14)
C	channel perimeter, m
C_1,..., C_4	constants of the developed law of the saturation index evolution, eq. (25)
D	determinant of the matrix A_{ij}
e	specific internal energy, J kg^{-1}
F	gravity force per two-phase mixture unit volume, N m^{-3}
h	specific enthalpy, J kg^{-1}
k	number of equations/(independent variables) in eq. system (14)
M	Mach number
N_i	i-th secondary determinant of eq. system (15)
m	mass flow rate, kg s^{-1}
n	exponent defined in eq. (32)
p	pressure, Pa
Q	stream of external heat transfer per two-phase mixture unit volume, W m^{-3}
q	heat flux density, W m^{-2}
s	specific entropy, J kg^{-1} K^{-1}
T	temperature, °C
t	dummy parameter (independent variable in eq. 15)
v	specific volume, m^3 kg^{-1}
w	velocity, m s^{-1}
x	quality/vapour mass fraction
y	saturation index
z	coordinate in flow direction, m

Greek symbols

α	nozzle divergent part angle, deg
Δ	used before a quantity symbol denotes a change in the quantity
δ	discrepancy between experimental and calculated pressure, $\delta=p_{exp}-p_{calc}$, *MPa*
θ	reduced subcooling level defined in eq.(27)
σ	standard deviation
σ_i	velocity-state vector in eq. (14)
ρ	density, kg m^{-3}
τ	wall shear stress, Pa
φ	function defined in eq. (30)

subscripts

0	intersection point of the calculated fluid expansion curve with the saturated liquid line
c	fluid critical point
conv	convergent part of the nozzle
div	divergent part of the nozzle
ml	metastable liquid fraction
in	nozzle inlet
ref	referential value
S	singular point (z_t<z<z_{out}, M = 1)
s	saturated
sg	saturated vapour
sl	saturated liquid
t	nozzle throat
out	nozzle outlet

motive nozzle making strong difficulties to accurately predict critical mass flow rate through the motive nozzle. The appearance and growth of vapour bubbles drastically decreases the fluid density. Consequently, the velocity, Mach number and fluid compressibility dramatically increase. However, due to the presence of dissipative phenomena, the flow achieves the local sound speed (M=1) somewhere after the nozzle throat. The further decompression and Mach number increase take place in the divergent portion of the nozzle.

Besides nozzles, the flashing phenomenon is encountered in such common devices as valves, orifices and throttling devices. Therefore, the accurate prediction of the flashing process is of crucial importance for a design of apparatus that could be generally classified as devices of chemical and process engineering. Cases of such applications were described for example by Pangarkar (2017),

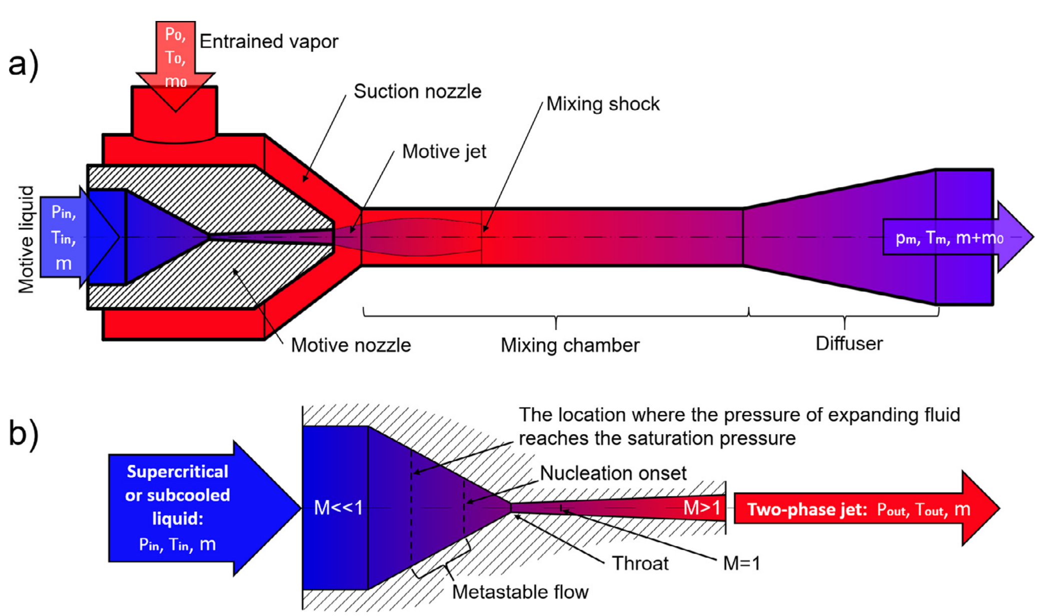

Fig. 1. Physical situation: a) two-phase ejector; b) flashing process in the convergent-divergent nozzle.

Weber et al. (2018), Rahman et al. (2010), Gamisans et al. (2004). The flashing also occurs in accidentally/randomly appearing channels (or microchannels) as cracks or full bore ruptures in pressurized tanks and tubes. Thus, the process is also relevant for nuclear power plant and chemical plant safety where the accurate prediction of the leakage rate through the crack plays a crucial role. These problems were, in turn, investigated, for example, by Hanaoka et al. (1990), Bartosiewicz et al. (2010), Papini et al. (2011).

As a result of this huge range of process occurrence, the flashing flow became a topic of many types of research and many modelling approaches have been developed. Those approaches can be classified mainly in three groups: lumped-parameter models, one-dimensional models and CFD approaches, as noted by Lorenzo et al. (2017). Unfortunately, the vast majority of those approaches were developed for water. However, the recent studies on implementations of the ejector in CO_2 systems such as heat pumps, refrigeration and air-conditioning devices, demonstrated significant improvement of those systems energy efficiency, as reported for example by Boccardi et al. (2017), Liu et al. (2016), Lucas et al. (2013). As a result, additional studies of carbon dioxide ejector refrigeration cycles have been conducted. Some of them included investigations on flashing flow through the convergent-divergent nozzle, e.g. Banasiak et al. (2013), Nakagawa et al. (2009). Consequently, some experimental data in this field are available providing an opportunity to study the predictions of CO_2 two-phase transonic flows through the convergent-divergent nozzles.

Among all aspects of the flashing flow, the problem of accurate predictions of critical mass flow rate is currently the most widely studied. The most profound conclusion from these studies is that the aspects of mechanical non-equilibrium are in this matter a secondary meaning issue. This was first concluded through theoretical considerations, among others, by Boure et al. (1976) and Bilicki et al. (1990). However, there are also empirical observations stating that the flashing transonic flow has usually form of a fully dispersed flow, Brown et al. (2013). Consequently, application of a complex two-fluid models or even simpler slip ratio models in modelling of the flashing transonic flow is unjustified. The problem of accurate predictions of the critical mass flow rate can be reduced to a problem of obtaining a physically consistent prediction of the sound speed, as inferred by Bilicki et al. (1990), Attou et al. (1999), Lorenzo et al. (2017). The mentioned researchers investigated various types of non-equilibrium two-phase flow models. Despite they used different analytical approaches, they all have shown that the physically consistent predictions of the sound speed cannot come from equilibrium approaches and that the introduction of the thermal non-equilibrium effects into the modelling is in this matter crucial. Keeping this in mind, the authors focused their attention first on the Homogeneous Relaxation Model (HRM) which is a relatively simple approach accounting for thermal non-equilibrium effects, Angielczyk et al. (2010). Using the HRM, the authors calculated the decompression curves for the selected nozzle geometries and boundary conditions obtaining reasonable matching with the applied experimental data. However, subsequently Bartosiewicz et al. (2010) proved that the Delayed Equilibrium Model (DEM), which is also a relaxation model, is more accurate than HRM in terms of the critical mass flow rate prediction. The ability of the DEM to accurately predict the critical mass flow rate was also confirmed by Lorenzo et al. (2017) through confrontation with experimental data of a wide range (incorporating flows through long tubes, short tubes, and slits) that comes mainly from the famous Super Moby-Dick experiment (this experiment is still the most coherent experimental database concerning water transonic flashing flows; it contains information on critical mass flow rates, pressure distributions and void fraction distributions). The main conclusion of the above-mentioned investigations is that among tested models (HEM, HRM and lumped-parameter approaches of Moody and Hanry-Fauske), DEM is the most accurate in terms of both the critical mass flow rate predictions and pressure distribution predictions. Moreover, the DEM has been implemented in WAHA code by Bartosiewicz and Seynhaeve (2014) and in NEPTUNE_CFD code by Duponcheel et al. (2013). It was shown that the use of DEM in CFD codes allows a very good representation of the experimental data and the results obtained were very close to the ones obtained by application of the stationary version of the model. Therefore, the main aim of the subsequent investigation, Angielczyk et al. (2019), was to check if the Delayed Equilibrium Model with a closure law, originally developed for water, may be considered as suitable for modelling of CO_2 transonic two-phase flows. Unfortunately, the mentioned investigations revealed that the original DEM closure law is not suitable for CO_2 transonic flow calculations. The investigation revealed also that the applied Darcy friction factor approach has a significant impact on the simulation results. Hence, two friction factor approaches were tested, namely, the Lockhart–Martinelli and the Friedel method. It was shown that the Lockhart–Martinelli approach returns such high values of the frictional pressure gradient that the obtained results have no physical meaning. In the case of the Friedel approach, this situation happened rarely. Therefore, the Friedel approach seemed to be more proper for CO_2 flows. Also, Aakenes et al. (2014) got a similar conclusion: among the investigated approaches (homogeneous friction-model, Friedel and Cheng approach), the Friedel approach turned out to be the most accurate for the case of CO_2 tube flows. Therefore, the authors decided to use the Friedel approach as a basis for developing a CO_2 dedicated approach. In the case of the saturation index evolution law, it was decided to develop a new formula on the basis of the original law.

The comparison of the proposed DEM setup with another DEM implementation is not possible since the developed approaches are the first proposition in the domain of DEM simulations of pure-CO_2 flows. Thus, the Homogeneous Equilibrium Model is applied as a reference case. Moreover, since the HEM does not consider any of non-equilibrium effects, its application as a comparative case allows to assess how the introduction of the thermal non-equilibrium effects affects prediction abilities of the modelling.

2. Modelling of one-dimensional stationary flashing flow in horizontal channel of varying cross-sectional area

2.1. Homogeneous Equilibrium Model (HEM)

Among the two-phase flow models, the HEM is distinguished by the smallest number of the closure equations. Namely, it requires only the equation for the transferred heat flux q and the equation for the wall shear stress τ. It is also related to an instantaneous mass transfer between fluid fractions. For those reasons, HEM is commonly treated as the reference case.

The HEM imposes the thermal equilibrium between vapour phase and liquid phase. Consequently, the temperatures and pressures of both phases are equal. It also assumes that phases are uniformly distributed (perfectly mixed), that results in equal velocities and mechanical equilibrium. The model consists of three conservation equations of mass, momentum, and energy, respectively:

$$w\frac{d\rho}{dz} + \rho\frac{dw}{dz} = -\rho w\frac{1}{A}\frac{dA}{dz}, \tag{1}$$

$$\frac{dp}{dz} + \rho w\frac{dw}{dz} = -\frac{\tau C}{A}, \tag{2}$$

$$\rho w\frac{dh}{dz} - w\frac{dp}{dz} = w\frac{\tau C}{A} + \frac{qC}{A} \tag{3}$$

The mass and momentum equations (1-2) can be easily derived from the non-stationary forms of the corresponding conservation laws, e.i. from equations given in the book of Städtke (2006). Also, the energy conservation in the form (3) can be derived from the time-dependent form, Städtke (2006):

$$A\frac{\partial}{\partial t}\left[\rho\left(e+\frac{w^2}{2}\right)\right]+\frac{\partial}{\partial z}\left[\rho wA\left(e+\frac{p}{\rho}+\frac{w^2}{2}\right)\right]=QA+wFA, \tag{4}$$

but the derivation requires some not necessarily obvious steps. First, it has to be noticed that $e+p/\rho$ is the definition of the specific enthalpy h and that, due to assumed flow stationarity, the term containing the time derivative, is equal to 0. Subsequent differentiation and taking into account that (in case of the horizontal flow) the term related to the work of the gravity force wFA vanishes, leads to the following form of the energy equation:

$$\rho w\frac{dh}{dz}+\rho w^2\frac{dw}{dz}=Q \tag{5}$$

Finally, replacement of the term containing dw/dz with an expression obtained from the momentum equation (2) and including that Q (the stream of the external heat transfer per unit mixture volume) can be expressed in terms of the heat flux q, gives the eq. (3).

The equations (1-3) have to be supplemented with the following state equations describing the specific volume (or density) and the specific enthalpy of the two-phase mixture:

$$v=\rho^{-1}=(1-x)v_{sl}+xv_{sg}, \tag{6}$$

$$h=(1-x)h_{sl}+xh_{sg} \tag{7}$$

Since the quantities with subscript sl and sg represent saturated liquid and saturated vapour properties, respectively, which are functions only of the pressure p, then the system contains three independent variables. Those three variables could be freely selected. In the implementation of HEM used in this investigation, the independent variables are: the pressure p, the quality (the saturated vapour mass fraction) x, and the velocity w. Since the flow is assumed to be adiabatic then the heat flux q is equal to 0.

2.2. Delayed Equilibrium Model (DEM)

The DEM assumes existence of three fractions: the metastable liquid phase (subscript ml), the saturated liquid phase (subscript sl), and the saturated vapour phase (subscript sg). The saturated fractions are in thermal equilibrium so that they have equal pressures and temperatures. The metastable fraction is assumed to have the same pressure as the saturated phases but higher temperature, as it is usually assumed to be frozen or proceed an isentropic expansion. Therefore, DEM takes into account the thermal non-equilibrium effects but it does not include the mechanical non-equilibrium effects. DEM consists of the conservation equations (1-3) substituted with the following state equations:

$$v=(1-y)v_{ml}+(y-x)v_{sl}+xv_{sg}, \tag{8}$$

$$h=(1-y)h_{ml}+(y-x)h_{sl}+xh_{sg} \tag{9}$$

On the basis of eq. (8) and eq. (9) there can be inferred that the saturation index y is simply the mass fraction of the saturated phases, thus it depends on three mass flow rates:

$$y=\frac{m_{sl}+m_{sg}}{m_{ml}+m_{sl}+m_{sg}}=\frac{m_{sl}+m_{sg}}{m} \tag{10}$$

In order to complete the model a mass balance equation for one of the three phases has to be added to the system of equations (1-3, 8-10). Therefore, the DEM model requires three closure equations describing: the wall shear stress τ, the heat flux q and the evolution law of the saturation index.

Originally, DEM was developed in purpose to simulate choked two-phase water flows. Thus, the original closure equation describes the evolution of water saturated fractions during the flashing process. Recently, the closure equation has been presented by Seynhaeve et al. (2015) and Lorenzo et al. (2017) in the following form:

$$\frac{dy}{dz}=\left(C_1\frac{C}{A}+C_2\right)(1-y)\left[\frac{p_s(T_{ml})-p}{p_c-p_s(T_{ml})}\right]^{C_3},$$

$$C_1=0.008390,\quad C_2=0.633691,\quad C_3=0.228127 \tag{11}$$

The implementation of DEM applied in this investigation treats the flow as adiabatic (q=0). The metastable fraction is subjected to an isentropic expansion. The independent variables are: p, x, y, w.

In the case when DEM simulation starts from the initial conditions containing: y=1, and operates with the following saturation index evolution law: $dy/dz=0$, then it is identical with HEM. Therefore, the proper evaluation of how the applied law of the saturation index evolution affects the simulation results should be based on a comparison with referential HEM data.

2.3. Modelling of subcooled liquid, supercritical fluid and saturated fractions properties

The titular data were obtained by an application of CoolProp library subroutines Bell et al. (2014). The application of Coolprop library allows to use the developed simulation code for all (123) fluids supported by Coolprop. Both Coolprop and the developed code are written in C++, which should benefit in the possibly shortest computational time. However, the issue of properties' accuracy has to be considered for each fluid separately. In the case of CO_2, the Coolprop subroutines apply an equation of state (EOS) developed by Span and Wagner (1996). This equation (SW EOS) is formulated in terms of reduced Helmholtz energy and covers the carbon dioxide properties from the triple point up to 800 MPa and 1100 K Span and Wagner (1996). Ameli et al. (2017) examined different well-known EOS models (SW, Peng-Robinson, Soave-Redlich-Kwong and the ideal gas equation) in a wide range of CO_2 state parameters (including the vicinity of the critical point) and compared the obtained results to the experimental data. They concluded that among the investigated models SW EOS showed the best accuracy. Therefore, in the case of CO_2, the application of the Coolprop subroutines is also beneficial in terms of accuracy.

2.4. Modelling of metastable liquid fraction properties

The specific enthalpy of the metastable fraction can be modeled based on the first law of thermodynamics in a form: $dh = vdp + Tds$. This form needs to be integrated from conditions determined by the intersection point of the calculated subcooled fluid expansion curve with the saturated liquid line (diamond points in Fig. 2), up to conditions given by the mixture pressure p and temperature of the metastable liquid T_{ml}. The properties in the mentioned intersection point are denoted with subscript 0 thus the specific enthalpy of the metastable fraction is given by the following formula:

$$h_{ml}(p,T_{ml})=h_0+\int_{p_0}^{p}\left[v_{ml}+T_{ml}\frac{\partial s_{ml}}{\partial p}\right]dp. \tag{12}$$

It is worth to notice that calculation of the specific enthalpy, with the above formula, requires utilization of a state equation to determine v_{ml} for given p and T_{ml}. As well as, additional assumptions/relations for calculating T_{ml} and $\partial s_{ml}/\partial p$. In this study, it was assumed that the metastable liquid fraction is subjected to an isentropic expansion (thus $\partial s_{ml}/\partial p=0$) and that it is incompressible

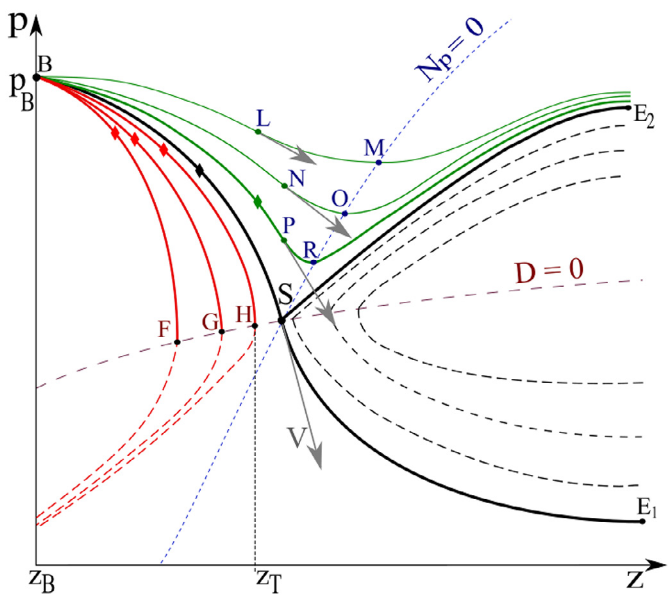

Fig. 2. Projection of solutions to the initial-value problems on p - z plane.

(v_{ml}=v_0), as a result, the metastable fraction specific enthalpy is a function of only pressure *p:*

$$h_{ml}(p) = h_0 + \int_{p_0}^{p} v_0 dp = h_0 + v_0(p - p_0). \tag{13}$$

The last required property, for conducting the modelling calculations, is the metastable fraction temperature T_{ml}. In general, it can be determined by using an equation of state in a process of searching for an isotherm of subcooled liquid that passes through a point determined by p and v_{ml} (or h_{ml}). In this study, an application of a linear extrapolation of subcooled liquid isotherms into the two-phase region is utilized (this procedure is analogical to a procedure, of extrapolation of subcooled liquid isochores into the two-phase region, described by Angielczyk et al., 2010). Those extrapolations require data on fluid properties at the liquid saturation line and in the subcooled liquid region. Those data were obtained by an application of subroutines of the CoolProp library. The library is briefly described in the previous Subsection.

3. Solution procedure

In the case of the nozzle fed with fluid under supercritical or subcooled state, in order to obtain the solution describing the nozzle flow, a single-phase flow model has to be utilized first. The applied single-phase flow model consists of the system of equations (1-3) supplemented with the thermodynamic state equations that describe the supercritical or subcooled properties of the fluid (Subsection 2.3). This model operates until the saturation conditions are reached. Subsequently, a two-phase flow model (e.g. HEM or DEM) has to be applied.

Each of the described flow models can be written in a form of the following nonlinear ordinary first-order differential equation system (Einstein summation convention has been applied, Bilicki et al., 1987):

$$A_{ij}(\sigma)\frac{d\sigma_i}{dz} = b_i(z, \sigma), \quad (i, j = 1, 2, ..., k) \tag{14}$$

The size and elements of the matrix A and the vector b depend on the model. The vector σ consists of k quantities describing the thermodynamic state of the fluid, and if necessary, the velocity of the fluid. The system (14) supplied with vector $\sigma_B = [\sigma_{1,B}, \sigma_{2,B}, ..., \sigma_{k,B}]^T$ (describing the nozzle inlet conditions) creates an initial-value problem, Press et al. (2002). A solution to the problem is a trajectory $\sigma(z)$ in $k+1$ dimensional phase space Ω, Bilicki et al. (1987). An approximation of this trajectory can be determined through numerical forward-marching integration of eq. system (14) from the inlet conditions towards the nozzle outlet. In order to conduct the integration, for example, Euler or Runge-Kutta method could be applied. However, an adaptive integration step version of the integration algorithm is recommended for accuracy reasons, Press et al. (2002). The form of eq. system (14) is inconvenient for numerical integration. Therefore, it is usually transformed, by application of Cramer's rule and introduction of a dummy parameter t, into the following autonomous form Bilicki et al. (1987), Press et al. (2002):

$$\left[\frac{dz}{dt}, \frac{d\sigma_1}{dt}, \frac{d\sigma_2}{dt}, \cdots, \frac{d\sigma_k}{dt}\right]^T = [D, N_1, N_2, \cdots, N_k]^T \tag{15}$$

where D denotes a determinant of the A matrix, and N_i are determinants of matrices created by replacing the j-th column of the matrix A with the vector b. Fig. 2 presents a projection of trajectories corresponding to flows through a convergent-divergent nozzle on pressure p - spatial coordinate z plane (σ_1=p, $\sigma_{1,B}$=p_B). The inlet conditions related to those flows differ only in the velocities. Consequently, all trajectories related to the curves in Fig. 2 start from the same values of the spatial coordinate z_B, the inlet pressure p_B, density ρ_B, and specific enthalpy h_B. Segments of the curves between the inlet point B and the diamond points represent single-phase liquid flows obtained by integration of the eq. system of the single-phase model. Consequently, after each diamond point, a two-phase flow model has to be applied in the integration process. The trajectories represented by curves passing through point M and O, do not reach the saturation liquid line (thus, there are no diamond points on those trajectories). Therefore, those trajectories represent single-phase flows and only the single-phase flow model is required to determine them. Each of the points: F, G, H is a point of maximum spatial coordinate at a related trajectory. Therefore, in each of these points dz/dt=0 (eq. 15), consequently they lie on the curve D=0 (the brown dashed line in Fig. 2). The physical interpretation of points at which D=0 is that at these points the fluid velocity is equal to the local speed of sound, Bilicki et al. (1987), Städtke (2006). Each of the points: M, O, R is a point of minimum pressure at a related trajectory. Therefore, in each of these points dp/dt=0, consequently, they lie on the curve N_p=0 (the blue dashed line in Fig. 2). Any trajectory that does not pass through the intersection point of the curves D=0 and N_i=0 can be determined through numerical forward-marching integration of eq. system (15) since at each point of such trajectory, the existence and uniqueness theorem is satisfied Bilicki et al. (1987), Press et al. (2002). However, it is worth to mention that having D=0 and any of Ns equal to zero, at a given point, means that also the remaining Ns are equal to 0 at this point, Bilicki et al. (1987). The trajectory that passes through the points B, E_1 and the mentioned intersection point S is the sought transonic solution (Fig. 2). According to eq. (15): $dz = D\ dt$ and $d\sigma_i = N_i\ dt$. Therefore, at the point S, the values of Δz and $\Delta\sigma_i$ calculated by the numerical integration methods are equal to zero regardless of the integration step size Δt. It means that the numerical integration algorithms cannot neither "start from" nor "pass through" this kind of points. In other words, at this kind of points either the uniqueness theorem or existence theorem is unsatisfied and those points are called singular points.

In summary, in the case of the transonic solutions determination, the forward-marching integration methods are inadequate and a more complex approach is required. The conventional solution to this problem arises from the theory of dynamical systems and was described by Bilicki et al. (1987), Bilicki et al. (1990), De Sterck (2009) and Angielczyk et al. (2019). However, a faster approach, that was detailed described by Angielczyk et al. (2019), was applied in this study. Here, the approach is presented in a very concise form that supposed to provide the reader with the knowledge required to understand the general concept.

The applied approach requires some information that can be obtained by conducting the Possible-Impossible flow algorithm (PIF), Boure et al. (1976), Attou et al. (1999), Lorenzo et al. (2017), Angielczyk et al. (2019). Namely, in each PIF iteration, a trajectory is determined (by numerical forward-marching integration) that can be categorized as an Impossible Flow trajectory (IF, the red curves in Fig. 2) if it crosses the *D=0* curve or Possible Flow trajectory (PF, the green curves in Fig. 2) if otherwise. Each subsequently determined trajectory passes closer to the sought transonic trajectory than the previously found trajectory of the same type (either IF or PF). Thus, the considered singular point approximation can be determined (providing that at least two IF trajectories have been found via the PIF iterations) in the following steps:

- Approximate the curve $D(\sigma) = 0$ by the straight line passing through point *G* and *H*.
- Determine a point $S_i(z_i,\sigma_i)$ that lies on the line. At this point $z_i=z_H+\Delta z$. Assume that $m_i=m_H+\Delta z(m_H\text{-}m_G)/(z_H\text{-}z_G)$.
- Use the gradient descent method (take S_i as a starting point) to determine $S_{i0}(z_i,\sigma_{i0})$ where $D = 0$, Press et al. (2002).
- If all *N*s at the point S_{i0} have different signs than in the point *H*, then repeat the previous steps with smaller Δz until the required accuracy is reached. Otherwise, repeat the previous steps but use *H* instead of *G* and S_{i0} instead of *H*.

The next step is to find the trajectory that passes through the determined singular point. However, as it was explained above, the numerical integration cannot start from the singular point. Nevertheless, if we could determine direction of a vector tangent to the trajectory at the singular point (direction of the vector *V* in Fig. 2) then making a step along this direction determines a point that is eligible for starting numerical integration. The up-stream integration (when it reaches z_B), determines the approximation of the inlet conditions *B* corresponding to the considered singular point. Similarly, down-stream integration determines the approximation of the outlet conditions E_1. An idea of how to obtain an approximation of the mentioned direction comes from the following consideration.

Fig. 2 shows the points *L, N, P* that are inflection points of the PF trajectories. The grey arrows represent vectors that are tangent to the trajectories at corresponding inflection points. The points *M, O, R* represent local pressure minima. It is crucial to notice that the closer to the point *S* the PF trajectory lies, the closer the inflection point of this trajectory is to the pressure minimum point of this trajectory. Finally, at the transonic trajectory those points merge into point *S*. Consequently, the direction of *V* can be approximated by the direction of the vector tangent to the last-found PF trajectory at its inflection point. The higher number of PIF iterations, the smaller distance between points *R* and *S* and the better approximation of the sought direction. The obtained direction can be directly used to carry out the integration from the considered singular point resulting with an approximation of the subsonic and supersonic parts of the sought transonic trajectory. Nevertheless, the higher accuracy can be reached by using the obtained approximation as a first guess for well-known iterative methods of eigenvector determination, e.g. inverse power method, Press et al. (2002).

4. The proposed law of the saturation index evolution

The flashing process occurs due to the static pressure drop below the saturation pressure in the flowing fluid. Therefore, the pressure drop rate determines the intensity of the phase change process that takes place in the expanding fluid. For the incompressible flows through channels with a constant cross-sectional area, the pressure drop occurs as a result of friction between the fluid layers (or elements) and between the fluid and the channel walls. However, in the case of the convergent-divergent nozzles, the additional decrease in the static pressure occurs due to the change in the cross-sectional area of the channel. Moreover, the nozzle is usually designed in such a way that the pressure decrease induced by the change of the cross-sectional area is much higher than the frictional pressure drop (short nozzle with high convergence).

The understanding of how the cross-sectional area change causes the static pressure change comes from an analysis that starts with the momentum conservation, eq. (2), which here is rewritten in a slightly different form:

$$\frac{dp}{dz} = -\rho w \frac{dw}{dz} - \frac{\tau C}{A}. \tag{16}$$

Thus, the total static pressure gradient is a sum of the accelerational pressure gradient (the first term) and the frictional pressure gradient (the second term). As it was explained above, in the considered case, the frictional pressure gradient can be omitted. Therefore:

$$\frac{dp}{dz} = \left(\frac{dp}{dz}\right)_{accelerational} = -\rho w \frac{dw}{dz}. \tag{17}$$

Replacement of the term that contains the velocity gradient (*dw/dz*) by an expression derived from the continuity equation (1) results with the following relation:

$$\frac{dp}{dz} = \frac{\rho w^2}{A}\frac{dA}{dz} + w^2\frac{d\rho}{dz}. \tag{18}$$

Therefore, the total static pressure gradient is a sum of the term containing the rate of the cross-sectional area change (*dA/dz*) and the term containing the density gradient ($d\rho/dz$). The density can be treated as a function of the static pressure and the specific entropy and then:

$$\frac{d\rho}{dz} = \frac{\partial\rho}{\partial p}\frac{dp}{dz} + \frac{\partial\rho}{\partial s}\frac{ds}{dz}. \tag{19}$$

Consequently, eq. (18) takes the following form:

$$\frac{dp}{dz} = \left(1 - w^2\frac{\partial\rho}{\partial p}\right)^{-1}\left(\frac{\rho w^2}{A}\frac{dA}{dz} + w^2\frac{\partial\rho}{\partial s}\frac{ds}{dz}\right). \tag{20}$$

In general, the change of the density is caused by the static pressure change, the heat transfer from surroundings into the fluid and work of the friction forces. However, the flow in a short nozzle can be treated as adiabatic, Attou and Bolle (2000). If the friction effects are negligible, as was discussed above, the flow is also isentropic (*ds/dz=0*) and then:

$$\frac{dp}{dz} = \left(1 - w^2\frac{\partial\rho}{\partial p}\right)^{-1}\frac{\rho w^2}{A}\frac{dA}{dz}. \tag{21}$$

The last equation proves that, in the considered case, the static pressure gradient is determined mainly by the rate of the cross-sectional area change. Consequently, the flashing process intensity is determined by this rate. This conclusion was a motivation for development of the correlation describing the law of the saturation index evolution in a form that strongly depends on the nozzle convergence and divergence rates. Those rates are defined as follows:

$$\left(\frac{dA}{dz}\right)_{conv} = \frac{A_t - A_{in}}{z_t - z_{in}}, \tag{22}$$

$$\left(\frac{dA}{dz}\right)_{div} = \frac{A_{out} - A_t}{z_{out} - z_t}, \tag{23}$$

and the proposed saturation evolution law has the following form:

$$\frac{dy}{dz} = \left\{C_1 + C_2 \exp\left[C_3 \frac{\left(\frac{dA}{dz}\right)_{div} - \left(\frac{dA}{dz}\right)_{conv}}{\left(\frac{dA}{dz}\right)_{ref} - \left(\frac{dA}{dz}\right)_{conv}}\right]\right\} \times (1-y)\left[\frac{p_s(T_{ml}) - p}{p_c - p_s(T_{ml})}\right]^{C_4}. \tag{24}$$

The values of the constants proposed for CO_2 are presented below:

$$C_1 = 38 \quad \frac{1}{m}, C_2 = 1.291 \cdot 10^{-31} \quad \frac{1}{m},$$
$$C_3 = 75.28, C_4 = -0.22. \tag{25}$$

The form of the proposed evolution law is analogical to the evolution law developed for two-phase water flow. However, the first term of the product in eq. (24) is modified in comparison with the corresponding term in the original form of the evolution law, eq. (11). The term containing a ratio of the perimeter and the cross-sectional area (C/A), that appears in the original form of the evolution law, is supposed to take into account the heterogeneous nucleation at the wall. Consequently, C_2 was meant to introduce the impact of nucleation in the bulk of the flow. However, this concept is physically reasonable, unfortunately, in the case of CO_2 flashing, it could be realized only by the application of quite complex functions instead of constants C_1 and C_2. Those functions could be derived from nucleation theories. However, this kind of approach requires information on the nuclei population on the channel walls and in the fluid itself. The information on the nuclei population on the nozzle walls could be estimated on the basis of information about the nozzle material and roughness of its walls. Unfortunately, the experimental data used to adjust the correlation coefficients do not contain information on the roughness of the walls. Moreover, in order to properly analyse the roughness impact on the flashing process, many sets of nozzle geometry, that differ only in the roughness of the walls, have to be experimentally investigated. For those reasons, it was decided to use a more general approach based on the nozzle convergence and divergence rates together with an assumption that the nozzle walls are smooth. The theoretical justification of this generalized approach is presented at the beginning of this Section.

The proposed formulation may be considered as more general as it correlates dy/dz with dA/dz and as it was proven by eq. (21), in the case of the nozzle flow, dA/dz determines the pressure gradient dp/dz. The last one is a driving force of the flashing process in the analogical manner as the temperature gradient is a driving force of the heat conduction process.

In summary, the approach proposed in eq. (24) maybe applied for all cases of flashing nozzle flow providing that the coefficients C_1-C_3 were properly adjusted for the applied fluid and roughness of the nozzle walls. The proposed coefficients, eq. (25), maybe thought as valid for the case of pure-CO_2 flashing flows through smooth nozzles only.

5. The frictional pressure gradient

In the previous investigation, Angielczyk et al. (2019), and work of Aakenes et al. (2014) it was shown that among investigated approaches the Friedel frictional pressure gradient method turned out to be the most accurate for CO_2 flows. Therefore, the approach proposed here is based on the Friedel method:

$$\left(\frac{dp}{dz}\right)_{frictional} = \begin{cases} (a_1 + a_2)\left(\frac{dp}{dz}\right)_{Friedel} & if \quad M < 1 \\ \left(\frac{dp}{dz}\right)_{Friedel,S} \cdot cos\varphi & otherwise \end{cases} \tag{26}$$

The coefficient a_1 turned out to be strongly dependent on the reduced subcooling level:

$$\theta = \frac{T_{in} - T_0}{T_c}. \tag{27}$$

The following relationship is proposed for the discussed case of CO_2 flow:

$$a_1 = \begin{cases} 3.565 - cos^{-2}(1504 \cdot \theta) & if \quad \theta \le 4.2705 \cdot 10^{-4} \\ 1.127 \cdot 10^{-22} \cdot \theta^{-6.603} & otherwise \end{cases} \tag{28}$$

The second coefficient a_2 depends on the nozzle convergence and divergence rates as follows:

$$a_2 = 0.3 - 0.1\frac{\left(\frac{dA}{dz}\right)_{div} - \left(\frac{dA}{dz}\right)_{conv} - a_{g1}}{a_{g2}},$$

$$a_{g1} = 1.08659 \cdot 10^{-3} m, \qquad a_{g2} = 4.8085 \cdot 10^{-5} m \tag{29}$$

The formula used for Mach numbers greater than unity requires the following relations:

$$\varphi = arccos\left(\frac{\left(\frac{dp}{dz}\right)_{Friedel,ref}}{\left(\frac{dp}{dz}\right)_{Friedel,S}}\right)\left(\frac{z - z_S}{z_{ref} - z_S}\right)^{0.75} \tag{30}$$

$$\left(\frac{dp}{dz}\right)_{Friedel,ref} = \left[b + (1-b)\left(\frac{z_{out} - z_{ref}}{z_{out} - z_T}\right)^n\right]\left(\frac{dp}{dz}\right)_{Friedel,S} \tag{31}$$

The exponent in Eq. (25) depends on the cross-sectional area ratio:

$$n = 4\left|\frac{dA}{dz}\right|\left(\frac{dA}{dz}\right)_{ref}^{-1} \tag{32}$$

For the discussed case the referential divergence ratio $(dA/dz)_{ref} = 0.0801424 \cdot 10^{-4}\ m$ and the referential spatial coordinate is given in the following form:

$$z_{ref} = z_t + 0.72\,(z_{out} - z_t) \tag{33}$$

Finally, the b parameter is dependent on the reduced subcooling level as follows:

$$b = \begin{cases} -1 & if \quad \theta \le 0.0046 \\ 0 & if \quad \theta > 0.00085 \\ 0.05 - 3.777 \cdot cos(-1.1244 \cdot 10^3 \cdot \theta) + \theta^{-0.105} & otherwise \end{cases} \tag{34}$$

From eq. (26) it can be inferred that the frictional pressure gradient can be lower than zero at the supersonic portion of the flow. The physical meaning and justification of this fact are described at the end of next Section. However here, it is necessary to mention that whether the frictional grained gets below zero and how fast it goes towards negative values depends on b parameter defined in eq. (34). It can be concluded, from this relationship that for sufficiently high reduced subcooling level b=0 and then the frictional pressure gradient never gets below zero. For sufficiently low reduced subcooling levels b = -1 and then transition from positive to negative values is the fastest which agrees with the experimental data.

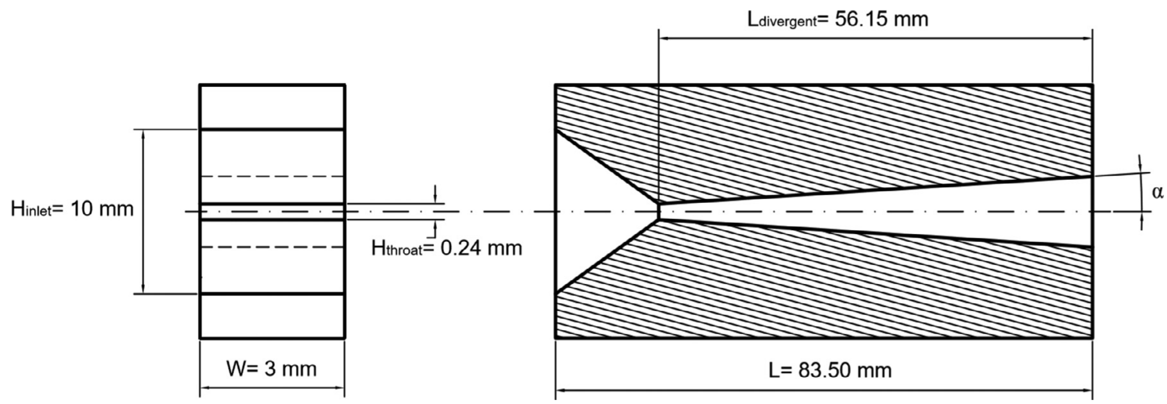

Fig. 3. Geometry of the experimental nozzle.

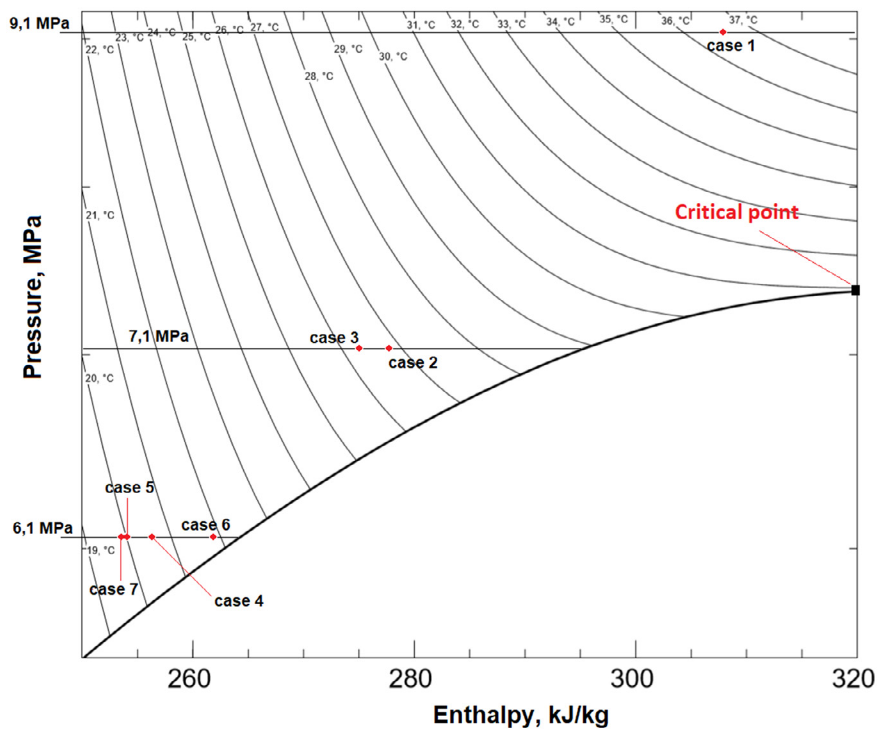

Fig. 4. Inlet conditions of the experimental cases in $p - h$ diagram.

6. The Experiment

The unique experimental data concerning two-phase transonic CO_2 flow through a de Laval nozzle were published by Nakagawa et al. (2009). The experiment was conducted as a blown-down test of CO_2. The investigated nozzle was fed from CO_2 tank and after passing through the nozzle and the back-pressure regulation valve, the fluid was exhausted to the atmosphere. Convergent-divergent stainless steel nozzles were applied in the experiment. All used nozzles had a rectangular cross-sectional area. The throat cross-sectional area was 0.24 mm by 3.00 mm rectangle. During all tests, the width of the nozzle (3.00 mm) and the lengths of convergent and divergent sections (27.35 mm, and 56.15 mm, respectively) were unchanged. The divergence angle α was changed, and for each nozzle geometry the pressure distribution in the divergent nozzle section was measured by means of four strain gauges. Also, the fluid temperature distribution was measured by means of nine taps. The geometry of the experimental nozzles is presented in Fig. 3 and Table 1.

Table 1
Variable parameters of the experimental nozzles.

Nozzle number	Divergent part angle α [rad]	Divergent part angle α [deg]	Outlet cross-section area [mm^2]
1	0.0013	0.077	1.17
2	0.0026	0.153	1.62
3	0.0053	0.306	2.52
4	0.0107	0.612	4.32

In summary, the experimental data consist of the static pressure distributions and the temperature distributions along the divergent part of each nozzle. Unfortunately, there is no data provided on the critical mass flow rates and the void fraction or the quality distributions.

The DEM postulates a perfect mixing of the fractions and that the metastable fraction temperature is higher than the temperature of the saturated fractions. Nevertheless, it does not define the

Table 2
Characteristics of the considered models.

Model	Applied approach of the frictional pressure gradient	Remarks
IHE	$(\frac{dp}{dz})_{frictional} = 0$	Homogeneous Equilibrium Model with $\tau=0$ (Isentropic Homogeneous Model)
HEM0	$(\frac{dp}{dz})_{frictional} = (\frac{dp}{dz})_{Friedel}$	Homogeneous Equilibrium Model with the original Friedel approach
DEM0	$(\frac{dp}{dz})_{frictional} = (\frac{dp}{dz})_{Friedel}$	Delayed Equilibrium Model with the original Friedel approach (*dy/dz* defined in Section 4)
DEM1	$(\frac{dp}{dz})_{frictional} = (a_1 + a_2)(\frac{dp}{dz})_{Friedel}$	Delayed Equilibrium Model (a_1 and a_2 defined in Section 5, *dy/dz* defined in Section 4)
DEM2	$(\frac{dp}{dz})_{frictional} = \begin{cases} (a_1+a_2)\left(\frac{dp}{dz}\right)_{Friedel} & if \quad M<1 \\ \left(\frac{dp}{dz}\right)_{Friedel,S} \cdot cos\varphi & otherwise \end{cases}$	Delayed Equilibrium Model with frict. approach defined in Section 5 (*dy/dz* defined in Section 4)

overall (or resulting) temperature, therefore, the experimental temperature distributions cannot be used to develop a new form of the saturation index evolution law and the frictional pressure drop gradient approach without introducing additional assumptions.

7. Analysis of simulation results

After the preliminary calculations, three out of ten experimental cases were excluded from the investigation as they turned out to be cases of a single-phase flow. Those three cases are related to the supercritical inlet conditions and the following nozzle divergent part angles: 0.077 °, 0.153 °, 0.306 °.

Therefore, the proposed approaches were developed on the base of seven experimental static pressure distributions of CO_2 two-phase transonic flows. The inlet conditions of the experimental flows and locations of those conditions with respect to the liquid saturation line are presented in Fig. 4.

Characteristic of the considered models are presented in Table 2. The leading idea, standing behind the selection of the model set, was to compare the predictive abilities of DEM equipped with different approaches of the frictional pressure gradient and the same, proposed in Section 4, law of the saturation index evolution. As reference data, simulation results of two HEM implementations were used. Namely, HEM equipped with the original Friedel frictional approach (HEM0) and the Isentropic Homogeneous Model (IHE) which assumes an adiabatic flow of inviscid fluid.

Since both the HEM0 and the DEM0 use the Friedel method, the comparison of their predictive abilities could indicate whether the proposed introduction of the thermal non-equilibrium effects, eq. (24), improves or deteriorates the obtained predictions. A comparison between DEM0 and DEM2 could be thought as the basis for the assessment of the proposed frictional approach impact. Finally, the simultaneous impact of both proposed approaches can be evaluated by comparison of results obtained with HEM0 and DEM2.

The selection of the IHE as a reference model is rooted in the findings of the previous investigation, Angielczyk et al. (2019). Namely, among investigated models, the IHE model gave the best predictions of the pressure distributions in the flow through nozzles with the highest divergent part angle (0.612 °). The DEM1 is required for further discussion of some features of the proposed frictional pressure gradient approach.

Table 3 presents the statistical results for each of the considered experimental cases. The statistics contain data describing (individually for each of the considered model) the maximal discrepancy between the experimental and calculated pressure values (δ_{MAX}), the mean value of the maximal discrepancies (δ_{MEAN}) and the standard deviation of the discrepancies (σ_δ).

Table 3
Statistical analysis of the experimental cases.

Model	$\|\delta_{MAX}\|$, MPa	δ_{MEAN}, MPa	σ_δ, MPa	*m*, kg/s
Case 1: p_{in}=9.1 MPa, T_{in}=36.5 °C, α=0.612 °				
IHE	0.437573	-0.14231	0.258558	0.02949
HEM0	0.312656	0.035875	0.239088	0.02945
DEM0	0.458329	0.309149	0.110721	0.03334
DEM1	0.326538	0.158008	0.126028	0.03348
DEM2	0.326606	0.161644	0.124409	0.03348
Case 2: p_{in}=7.1 MPa, T_{in}=26.7 °C, α=0.306 °				
IHE	1.321137	-0.63835	0.638678	0.02521
HEM0	1.007396	-0.31063	0.641623	0.02516
DEM0	0.614721	0.16060	0.409624	0.02790
DEM1	0.452387	0.012684	0.392827	0.02851
DEM2	0.41151	-0.02056	0.37060	0.02851
Case 3: p_{in}=7.1 MPa, T_{in}=26.4 °C, α=0.612 °				
IHE	0.313535	-0.17179	0.242914	0.02492
HEM0	0.357552	0.075028	0.267233	0.02491
DEM0	0.377476	0.12547	0.238878	0.02494
DEM1	0.287818	0.024647	0.247424	0.02506
DEM2	0.283189	0.025773	0.244647	0.02506
Case 4: p_{in}=6.1 MPa, T_{in}=20.5 °C, α=0.077 °				
IHE	1.500366	-1.22566	0.359981	0.02313
HEM0	0.481667	-0.06179	0.418865	0.02286
DEM0	0.623317	0.220239	0.290221	0.02338
DEM1	0.288211	-0.03774	0.229842	0.02513
DEM2	0.234554	-0.14376	0.076436	0.02513
Case 5: p_{in}=6.1 MPa, T_{in}=20 °C, α=0.153 °				
IHE	1.254498	-0.89547	0.266251	0.02347
HEM0	0.674583	-0.32414	0.282602	0.02342
DEM0	0.486728	0.231684	0.232676	0.02593
DEM1	0.346608	0.035739	0.246082	0.02721
DEM2	0.346608	-0.00973	0.256742	0.02721
Case 6: p_{in}=6.1 MPa, T_{in}=21.8 oC, α=0.306 °				
IHE	1.311872	-0.45435	0.819878	0.02238
HEM0	1.056922	-0.18955	0.820001	0.02232
DEM0	0.841639	0.120267	0.664492	0.02483
DEM1	1.24890	0.493003	0.706262	0.02365
DEM2	0.358027	-0.00823	0.323996	0.02365
Case 7: p_{in}=6.1 MPa, T_{in}=19.9 °C, α=0.612 °				
IHE	0.125272	0.018118	0.128694	0.02368
HEM0	0.390669	0.205722	0.15741	0.02356
DEM0	0.406573	0.240799	0.135744	0.02359
DEM1	0.178094	0.096743	0.100322	0.02369
DEM2	0.181938	0.100548	0.101773	0.02369

The relative discrepancies analysis is not applied since it is not reliable in cases when the measured quantity has a decreasing tendency (the relative error approaches infinity when the measured value approaches 0). Since the experimental data concern decompression processes, the described situation happens in each con-

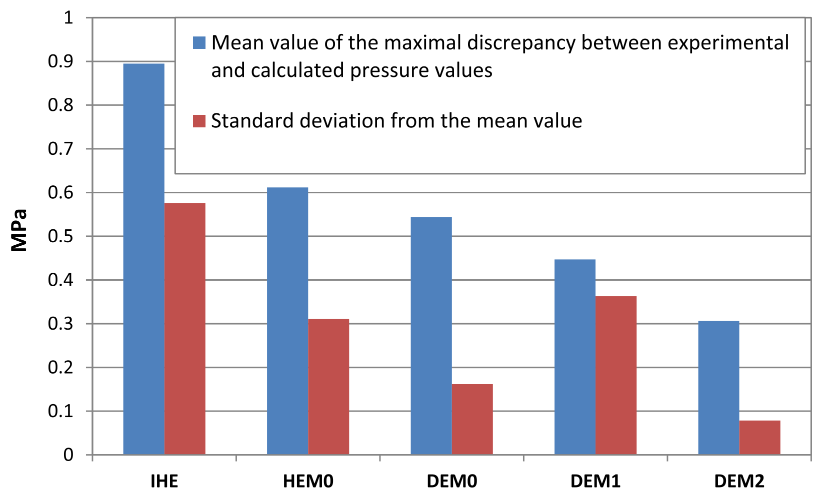

Fig. 5. The overall statistical analysis of each considered model.

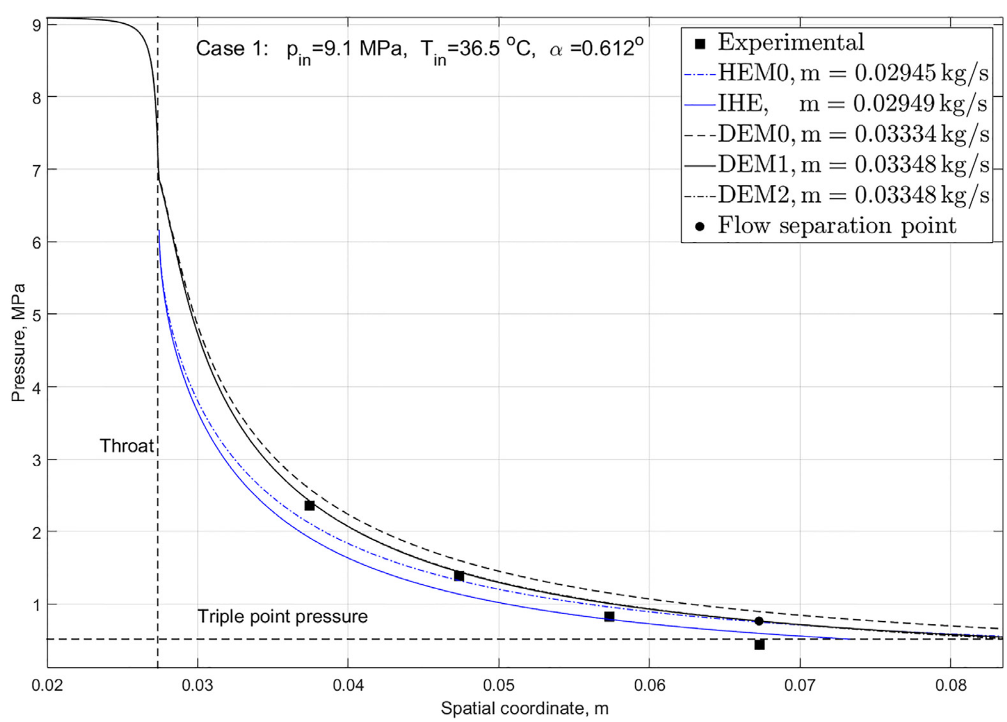

Fig. 6. Calculated pressure profiles of Nakagawa et al. blow-down CO_2 experiment for supercritical inlet conditions (Case 1: 9.1 MPa, 36.5°C).

sidered experimental flow and the tendency can be clearly seen in Figs 6–8. The measured pressure values decrease from very high values (even around 5 MPa) to very low values (even around 0.2 MPa). For these reasons, the absolute value of the maximal discrepancy between experimental and calculated pressure values was selected as a validation parameter.

The overall statistics (that cumulate data of all considered experimental cases) concerning the maximal discrepancy between experimental and calculated pressure values are presented in Table 4 or in Fig. 5, separately for each model.

A brief analysis of the data presented in Table 4 or in Fig. 5 reveals that the DEM equipped with the proposed approaches (DEM2) has the best prediction ability among the considered models. Namely, it is characterised by the lowest value of the mean maximum pressure discrepancy $|\delta_{MAX}|_{MEAN}$ with the lowest standard deviation from this value $\sigma_{\delta MAX}$. Moreover, the absolute value

Table 4
The overall statistical analysis of the considered models.

Model	$\lvert\delta_{MAX}\rvert_{MEAN}$, MPa	$\sigma_{\delta MAX}$, MPa	$\lvert\delta_{MAX}\rvert$, MPa
IHE	0.8949	0.5760	1.5004
HEM0	0.6116	0.3105	1.0569
DEM0	0.5441	0.1618	0.8416
DEM1	0.4469	0.3630	1.2489
DEM2	0.3061	0.0785	0.4115

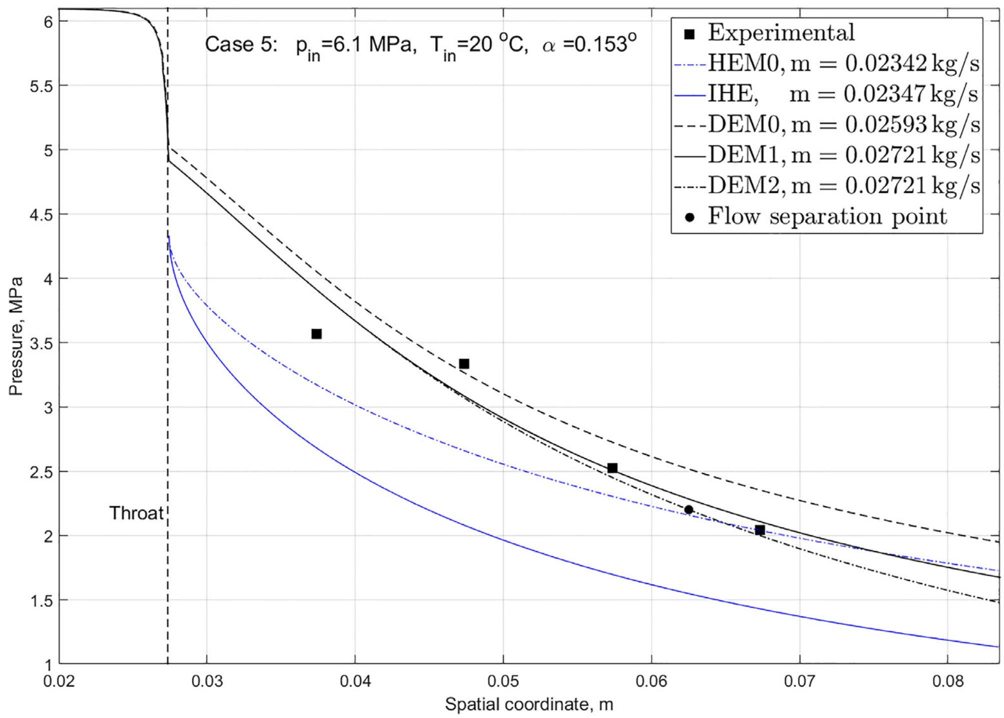

Fig. 7. Calculated pressure profiles of Nakagawa et al. blow-down CO_2 experiment for subcritical inlet conditions (Case 5: 6.1 MPa, 20°C).

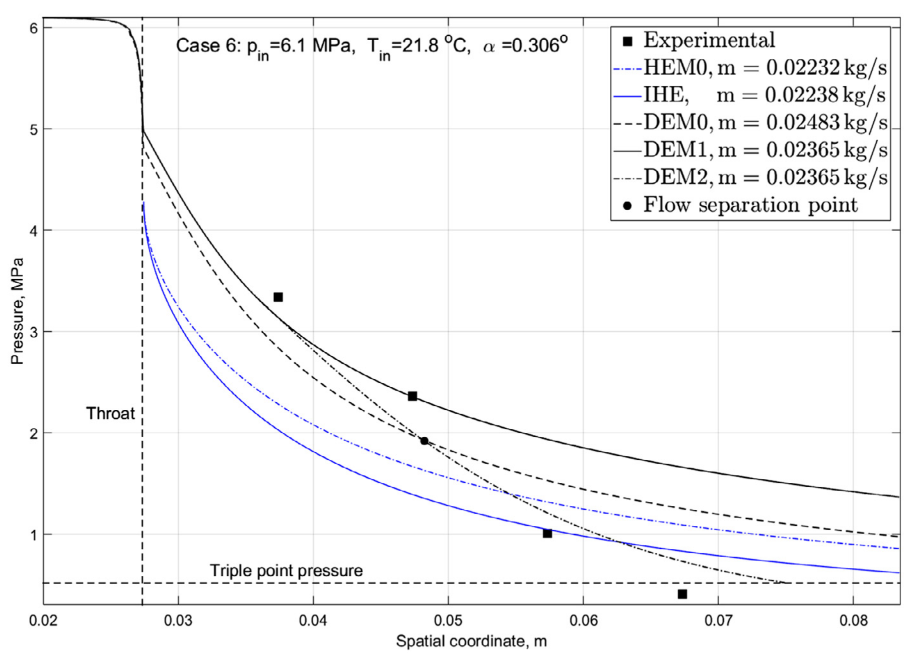

Fig. 8. Calculated pressure profiles of Nakagawa et al. blow-down CO_2 experiment for subcritical inlet conditions (Case 6: 6.1 MPa, 21.8°C).

of the maximum discrepancy $|\delta_{MAX}|$ is also the lowest for this model.

The comparison between HEM0 and DEM2 reveals that the introduction of both developed approaches strongly improved obtained results. The mean maximum discrepancy between experimental and calculated pressure values decreased almost 2 times but the standard deviation has decreased almost 4 times. While the maximal absolute discrepancy between experimental and calculated pressure values decreased 2.5 times.

The comparison between HEM0 and DEM0 reveals that the application of the developed saturation index evolution law decreased the mean maximum discrepancy between experimental and calculated pressure values approximately 1.12 times while the related standard deviation decreased 1.92 times.

The comparison between DEM0 and DEM2 reveals that the introduction of the developed frictional pressure gradient approach decreased the mean maximum discrepancy between experimental and calculated pressure values approximately 1.78 times while the related standard deviation decreased 2.06 times.

Figs. 6-8 present calculated and experimental pressure distributions for three representative flow cases. It can be seen that the DEM1 and the DEM2 pressure profiles are ideally overlapping until some point. It can be inferred from eq. (26) that at this point $M = 1$. Moreover, this point is localized between the nozzle throat and the nozzle outlet thus it is a singular point. Consequently, the related critical mass flow rate m has the same value for both distributions. Moreover, any changes that occur after this point cannot affect the upstream flow (this fact is important, since it can be a reason for an abrupt pressure gradient change in the middle of the nozzle diffuser, in cases similar to flows presented in Fig. 7 and Fig. 8). Finally, the considered distribution curves split because after the singular point each of the considered models uses other frictional pressure gradient formula.

It can be seen that each presented pressure profile of the DEM2 passes through a point denoted by a black circle and described as flow separation point (this kind of points do not occur on the DEM1 profiles and do not occur on all DEM2 profiles). At the mentioned points, the proposed frictional pressure gradient formula returns zero. Consequently, after this point, the frictional pressure gradient has a negative value. This situation can be physically justified only if at the mentioned point a separated flow forms. Namely, the boundary layer becomes detached from the nozzle diffuser walls and takes the structure of eddies and vortices. This phenomenon was reported, e.g. by Nussdorfer (1954), Bogdonoff and Kepler (1955), Ostlund (2005), Xiao and Papamoschou (2007), Papamoschou et al. (2008), Délery and Dussauge (2009), and has been even theoretically described, e.g. by Neiland (1969). However, the theory states that the described situation requires the existence of so-called adverse pressure gradient in the diffuser. In the case of supersonic flow, it means that a normal shock wave has to appear. The experimental data do not show any signs of such phenomena. However, it cannot be ruled out that the normal shocks (or in other words, initial subsonic regions) were not recorded since they appear between the last pressure gauge and the nozzle outlet (or even just before the backpressure regulation valve). Examples of diffuser transonic flows in which the flow separation starts far ahead of the appearance of the initial subsonic region were shown, in the form of Schlieren images, by Papamoschou et al. (2008). In such cases, the flow separation is induced by weak oblique shock waves. Therefore, the phenomenon is typical 3-dimensional (or at least 2-dimensional) issue and its capturing in the proposed 1-dimensional approach is some kind of averaged solution.

8. Conclusions

The presented statistical analyses proved that the proposed saturation index evolution law and the proposed frictional pressure gradient approach significantly improve the prediction ability of transonic flow pressure profiles of the Delayed Equilibrium Model: The mean maximum discrepancy between experimental and calculated static pressure values decreased almost 2 times, with the almost fourfold decrease in the standard deviation, in comparison to the referential Homogeneous Equilibrium Model. A comparison of the proposed DEM setup with another competitive DEM implementation is not possible since the developed law of the saturation index evolution is the first proposition in the domain of DEM simulations of pure-CO_2 flows. However, there are some propositions of CO_2 closure law for the Homogeneous Relaxation Model, Haida et al. (2018), as well as quasi-DEM formulations for CO_2-PAG oils mixtures, Banasiak et al. (2013). Thus, the comparative analysis of these thermal non-equilibrium two-phase flow relaxation models could be a topic of further investigation.

The IHE model can compete with proposed DEM setup on the prediction accuracy of the static pressure profiles of CO_2 transonic flows through nozzles with a high divergent part angle but it completely fails in case of nozzles with low and moderate angles of the divergent part (Table 3 and 4 and Angielczyk et al., 2019). This proves that the accurate prediction of CO_2 flashing flow cannot be obtained from equilibrium approaches and that the proper introduction of the thermal non-equilibrium effects into the modelling has significant importance.

The strong impact of the applied frictional pressure gradient approach on the simulation results has been already reported in the previous investigation, Angielczyk et al. (2019). It was shown that the Lockhart–Martinelli approach (and sometimes the Friedel method), applied to CO_2 flow simulations, returns so high values of the frictional pressure gradient that the obtained results have no physical meaning. In this study, it was additionally demonstrated that the replacement of the original Friedel approach by the proposed approach enhances the considered predictions even stronger than the introduction of the thermal non-equilibrium effects. It is very important conclusion since the issue of applied frictional pressure gradient method is commonly regarded as a secondary-meaning issue, which is evidenced by the fact that in the above-mentioned articles, on relaxation model closure laws, the applied frictional approaches were not even briefly described. One of the mentioned researches, Banasiak et al. (2013), compared a quasi-DEM approach, in which the saturation fractions evolution law was based on the nucleation theory, with the same experimental data as used in this investigation. However, significant inconsistencies have been revealed. Banasiak et al. (2013) inferred that the departure from the experimental data was due to the fact that the considered experiment concerns flows of pure-CO_2 while the applied evolution law was adjusted on the basis of their own experiment in which contamination of CO_2 with lubricant (PAG oil) was not negligible. Naturally, the influence of the lubricant contamination is not questioned here, however, in the light of the above-mentioned conclusion, the frictional pressure gradient influence should also be considered as a possible reason for the mentioned inconsistencies.

Acknowledgements

The research was carried out as part of research work No. WZ/WM-IIM/1/2020 at the Bialystok University of Technology and financed from a subsidy provided by the Ministry of Science and Higher Education.

References

Aakenes, F., Munkejord, S.T., Drescher, M., 2014. Frictional pressure drop for two-phase flow of carbon dioxide in a tube: Comparison between models and experimental data. Energy Procedia 51, 373–381 7th Trondheim Conference on CO2 capture, Transport and Storage (2013).

Ameli, A., Uusitalo, A., Turunen-Saaresti, T., Backman, J., 2017. Numerical sensitivity analysis for supercritical co2 radial turbine performance and flow field. Energy Procedia 129, 1117–1124 4th International Seminar on ORC Power Systems September 13-15th.

Angielczyk, W., Bartosiewicz, Y., Butrymowicz, D., Seynhaeve, J.-M, 2010. 1-D modelling of supersonic carbon dioxide two-phase flow through ejector motive nozzle. International Refrigeration and Air Conditioning Conference.

Angielczyk, W., Seynhaeve, J.M., Gagan, J., Bartosiewicz, Y., Butrymow-icz, D., 2019. Prediction of critical mass rate of flashing carbon dioxide flow in convergent–divergent nozzle. Chemical Engineering and Processing- Process Intensification 143, 107599.

Attou, A., Bolle, L., Seynhaeve, J., 2000. Experimental study of the critical flashing flow through a relief line: evidence of the double-choked flow phenomenon. International Journal of Multiphase Flow 26 (6), 921–947.

Attou, A., Seynhaeve, J., 1999. Steady-state critical two-phase flashing flow with possible multiple choking phenomenon part 1: Physical modelling and numerical procedure. Journal of Loss Prevention in the Process Industries 12, 347–359.

Bartosiewicz, Y., Giot, M., Seynhaeve, J.-M., 2010. Revisiting modelling techniques and validation experiments for two-phase choked flows relevant to loca. The 8th International Topical Meeting on Nuclear Thermal-Hydraulics, Operation and Safety (NUTHOS-8) N8P0317 Shanghai.

Bartosiewicz, Y., Seynhaeve, J.-M., 2014. Delayed Equilibrium Model (DEM) of flashing choked flows relevant to LOCA and implementation in system codes. ICONE22-30957, Prague, Czech Republic.

Banasiak, K., Hafner, A., 2013. Mathematical modelling of supersonic two-phase R744 flows through converging–diverging nozzles: The effects of phase transition models. Applied Thermal Engineering 51 (1), 635–643.

Bell, I.H., Wronski, J., Quoilin, S., Lemort, V., 2014. Pure and pseudo-pure fluid thermophysical property evaluation and the open-source thermophysical property library CoolProp. Industrial & Engineering ChemistryResearch 53 (6), 2498–2508.

Bilicki, Z., Dafermos, C., Kestin, J., Majda, G., Zeng, D., 1987. Trajectories and singular points in steady-state models of two-phase flows. International Journal of Multiphase Flow 13 (4), 511–533.

Bilicki, Z., Kestin, J., 1990. Physical aspects of the relaxation model in two-phase flow. Proceedings of the Royal Society of London A: Mathematical. Physical and Engineering Sciences 428 (1875), 379–397.

Boccardi, G., Botticella, F., Lillo, G., Mastrullo, R., Mauro, A., Trinchieri, R., 2017. Experimental investigation on the performance of a transcritical co2 heat pump with multi-ejector expansion system. International Journal of Refrigeration 82, 389–400.

Bogdonoff, S.M., Kepler, C.E., 1955. Separation of a supersonic turbulent boundary layer. Journal of the Aeronautical Sciences 22 (6).

Boure, J., Fritte, A., Giot, M., Reocreux, M., 1976. Highlights of two-phase critical flow: On the links between maximum flow rates, sonic velocities, propagation and transfer phenomena in single and two-phase flows. International Journal of Multiphase Flow 3 (1), 1–22.

Brown, S., Martynov, S., Mahgerefteh, H., Proust, C., 2013. A homogeneous relaxation flow model for the full bore rupture of dense phase CO_2 pipelines. International Journal of Greenhouse Gas Control 17, 349–356. doi:10.1016/j.ijggc.2013.05.020, In press.

De Sterck, H., 2009. Critical point analysis of transonic flow profiles with heat conduction. SIAM Journal on Applied Dynamical Systems 6 (3), 645–662 2007.

Délery, J., Dussauge, J.-P., 2009. Some physical aspects of shockwave/boundary layer interactions. Shock Waves 19 (6), 453.

Duponcheel, M., Seynhaeve, J.-M., Bartosiewicz, Y., 2013. Implementation and validation of the DEM model in NEPTUNE_CFD and its application to the simulation of double-choked flows. NURESAFE 22 report D3112a-b.

Gamisans, X., Sarr'a, M., Lafuente, F., 2004. Fluid flow and pumping efficiency in an ejector-venturi scrubber. Chemical Engineering and Processing: Process Intensification 43 (2), 127–136.

Haida, M., Smolka, J., Hafner, A., Palacz, M., Banasiak, K., Nowak, A.J., 2018. Modified homogeneous relaxation model for the R744 transcritical flow in a two-phase ejector. International Journal of Refrigeration 85, 314–333.

Hanaoka, Y., Maeno, K., Zhao, L., Heymann, G., 1990. A study of liquid flashing phenomenon under rapid depressurization. JSME international journal. Ser. 2, Fluids engineering, heat transfer, power, combustion, thermos physical properties 33 (2), 276–282.

Liu, F., Groll, E.A., Ren, J., 2016. Comprehensive experimental performance analyses of an ejector expansion transcritical CO_2 system. Applied Thermal Engineering 98, 1061–1069.

Lorenzo, M.D., Lafon, P., Seynhaeve, J.-M., Bartosiewicz, Y., 2017. Benchmark of delayed equilibrium model (DEM) and classic two-phase critical flow models against experimental data. International Journal of Multiphase Flow 92, 112–130.

Lucas, C., Koehler, J., Schroeder, A., Tischendorf, C., 2013. Experimentally validated co2 ejector operation characteristic used in a numerical investigation of ejector cycle. International Journal of Refrigeration 36 (3), 881–891.

Nakagawa, M., Berana, M.S., Kishine, A., 2009. Supersonic two-phase flow of co2 through converging–diverging nozzles for the ejector refrigeration cycle. International Journal of Refrigeration 32 (6), 1195–1202.

Neiland, V.Y., 1969. Theory of laminar boundary layer separation in super-sonic flow. Fluid Dynamics 4 (4), 33–35.

Nussdorfer, T. J. (1954). Some observations of shock-induced turbulent separation on supersonic diffusers.

Ostlund, B.M.-K., 2005. Supersonic flow separation with application to rocket engine nozzles. AIAA Journal 58 (3).

Pangarkar, V.G., 2017. Process intensification in multiphase reactors: From concept to reality. Chemical Engineering and Processing - Process Intensification 120, 1–8.

Papamoschou, D., Zill, A., and Johnson, A. (2008). Supersonic flow separationin planar nozzles.Shock Waves, 19(3):171.

Papini, D., Grgic, D., Cammi, A., Ricotti, M.E., 2011. Analysis of different containment models for iris small break loca, using gothic and relap5 codes. Nuclear Engineering and Design 241 (4), 1152–1164 International Conference on Nuclear Energy for New Europe 2009.

Press, W.H., Teukolsky, S.A., Vetterling, W.T., Flannery, B.P., 2002. Numerical Recipes in C++: The Art of Scientific Computing, volume 1002. Cambridge University Press, third edition.

Rahman, F., Umesh, D., Subbarao, D., Ramasamy, M., 2010. Enhancement of entrainment rates in liquid–gas ejectors. Chemical Engineering and Processing: Process Intensification 49 (10), 1128–1135.

Seynhaeve, J.-M., Crécy, A. D., and Bartosiewicz, Y. (2015). Uncertainty analysis of delayed equilibrium model (DEM) using the circe methodology. NURETH-16, Chicago, IL, August 30-September 4.

Span, R., Wagner, W., 1996. A new equation of state for carbon dioxide covering the fluid region from the triple-point temperature to 1100 k at pressures up to 800 MPa. Journal of Physical and Chemical Reference Data 25 (6), 1509–1596.

Städtke, H., 2006. Gasdynamic Aspects of Two-Phase Flow. WILEY-VCH, Verlag GmbH Co. KGaA..

Weber, S., Schaepe, S., Freyer, S., Kopf, M.-H., Dietzsch, C., 2018. Effect of ejector operation on the oxygen transfer in a pilot jet loop reactor. Chemical Engineering and Processing - Process Intensification 131, 43–50.

Xiao, H.M.T., Papamoschou, D., 2007. Numerical investigation of supersonic nozzle flow separation. AIAA Journal 45 (3).